Int. J. Therm. Sci. (2000) 39, 896–908

S1290-0729(00)01175-3/FLA

Burnout in subcooled flow boiling of water. A visual experimental study

Gian Piero Celata [a]*, Maurizio Cumo [b], Andrea Mariani [a], Giuseppe Zummo [a]

[a] *ENEA, Engineering Division, National Institute of Thermal Fluid-Dynamics, Via Anguillarese 301, S.M. di Galeria, 00060 Rome, Italy*

[b] *University of Rome La Sapienza, DINCE, Cso. Vittorio Emanuele II, 244, 00186 Rome, Italy*

(Received 19 May 2000, accepted 13 July 2000)

Abstract — The objective of the present work is to perform a photographic study of the burnout in highly subcooled flow boiling, in order to provide a qualitative description of the flow pattern under different conditions of boiling regime: ONB (onset of nucleate boiling), subcooled flow boiling and thermal crisis. In particular, the flow visualisation is focused on the phenomena occurring on the heated wall during the thermal crisis up to the physical burnout of the heater. Vapour bubble parameters are measured from flow images recorded, while the wall temperature is measured with an indirect method, by recording the heater elongation during all flow regimes studied. The combination of bubble parameters and wall temperature measurements as well as direct observations of the flow pattern, for all flow regimes, are collected in graphs which provide a useful global point of view of boiling phenomena, especially during boiling crisis. Under these conditions, a detailed analysis of the mechanisms leading to the critical heat flux is reported, and the so called events sequence, from thermal crisis occurrence up to heater burnout, is illustrated. © 2000 Éditions scientifiques et médicales Elsevier SAS

boiling / flow boiling / critical heat flux / visualization / bubbles / subcooling

Nomenclature

CHF	critical heat flux	$kW \cdot m^{-2}$
D_b	vapour bubble diameter or length	μm
D_h	channel flow hydraulic diameter	mm
G	mass flux	$kg \cdot m^{-2} \cdot s^{-1}$
k	thermal conductivity	$kW \cdot m^{-1} \cdot K^{-1}$
p	pressure	bar
ONB	onset of nucleate boiling	
q''	heat flux	$kW \cdot m^{-2}$
T_{in}	inlet temperature	°C
T_w	wall temperature	°C
T_l	liquid temperature	°C
u	velocity	$m \cdot s^{-1}$

Greek symbols

δ	vapour bubble thickness or height	μm
δ_v	vapour film thickness	μm
$\Delta T_{sub,in}$	inlet subcooling	K

* Correspondence and reprints.
celata@casaccia.enea.it

1. INTRODUCTION

Over the last forty years the interest of researchers toward boiling crisis and the relative critical heat flux (CHF) in subcooled flow boiling of water has been increasing due initially to the development of nuclear fission reactors and recently to thermonuclear fusion reactor requirements.

Subcooled flow boiling is a very efficient heat transfer regime for the cooling of those components which are subjected to very high heat fluxes, where the CHF, with the associate burnout of the heat transfer surface, represents an insurmountable limit for this efficient heat transfer technique.

Although the interest for the CHF is high, a detailed knowledge of the phenomena causing the boiling crisis on the heat transfer surface is scarce, and, in particular, there are still relevant disagreements, among researchers, about the mechanisms triggering the boiling crisis. Disagreements are caused by the fact that the direct observation of the heater surface during the boiling crisis, by means of flow visualisation, is very difficult because of

small vapour bubble dimensions, bubble crowding and high liquid velocity. Therefore, relatively few works on burnout visualisation were carried out in the past, and, in particular very few of them reported direct observations of the boiling phenomena at the CHF.

Gunther [1] carried out experiments in subcooled flow boiling of water (liquid velocity 4.8–40 $m \cdot s^{-1}$ and pressure 0.1–0.5 MPa) making direct observations of flow pattern at the CHF using high speed movies (up to 20 000 fps). He used a rectangular test section ($D_h =$ 6.93 mm and $Z = 152$ mm). He reported vapour bubbles parameter (radius, period of existence, density on the heater surface) as a function of time. At the boiling crisis he noted the formation of a local vapour film due to the bubbles coalescence. The passage of these long vapour films caused a reduction in the heat transfer on the heater surface, with associated wall temperature increase. At the CHF, with sufficiently high wall temperature increments, vapour films could spread, thus causing further temperature increases up to the heater burnout.

Kirby et al. [2–4] studied the CHF visualising the water subcooled flow boiling. They used, in [2], a square $25.4 \times 25.4\,mm^2$ cross sectional test section and, in [3, 4], an annular test section with a hydraulic diameter of 19 mm. Visual experiments were performed in a low pressure (0.1–0.17 MPa) and low liquid velocity (0.6–1.3 $m \cdot s^{-1}$) range. They found that the flow pattern in the channel at the burnout depended on the liquid subcooling, and vapour bubbles tended to keep to the heater surface. These authors suggested a CHF mechanism based on small dry spots formation under some nucleation bubbles.

Van der Molen and Galjee [5] studied experimentally CHF in water subcooled flow boiling, using an annular test section ($D_h = 6, 14, 24, 35$ mm, heated length $Z = 190$ mm). They obtained photographs and high speed films (3 000 fps) of flow pattern in low pressure (0.1–0.2 MPa) and low liquid velocity (1–2.5 $m \cdot s^{-1}$). Their flow pattern observations revealed the presence of slug flow with small hydraulic diameters ($D_h = 6$ and 14 mm), while with larger hydraulic diameters ($D_h = 24$ and 35 mm) the flow pattern was characterised by a thick bubbly layer. For increasing values of the heat flux delivered to the test section, the authors observed an increase in the bubbles population on the heater surface. They proposed two CHF mechanisms based on the wall temperature reaching the Leidenfrost value. In slug flow, after the passage of a slug there is a wall temperature increment. For a particular combination of heat flux, slug length and slug velocity, the wall temperature may reach the Leidenfrost value with the consequent heater burnout occurrence. When the flow pattern was characterised by the presence of a bubbly layer, at high heat flux, the radial growth of a vapour bubble was interrupted by the presence of neighbour bubbles. In this situation a small portion of liquid could be trapped among several bubbles and the evaporation of this liquid layer (called microlayer by the authors) led to the a wall temperature increment. For sufficiently long periods of the bubbly layer existence the wall temperature could reach the Leidenfrost value, with the consequent heater burnout.

Fiori and Bergles [6] described the physical phenomena occurring before and at the CHF in subcooled flow boiling of water. They used an annular test section ($D_h =$ 5.6 mm and heated length 254 mm) and performed visual experiments with water at low pressure ($p = 0.15$–0.3 MPa) and low velocity ($u = 0.5$–1.5 $m \cdot s^{-1}$) range. The flow pattern during the boiling crisis was of the slug flow type at low velocity and froth flow at high liquid velocity. According to the authors, the froth flow pattern was a sort of transition between slug flow and annular flow. They also measured the wall temperature and found an oscillatory behaviour for it at the CHF. In particular, they recorded a typical wall temperature increment during a vapour clot passage over the heater surface. During the vapour clot passage, a hot spot could form from the vaporisation of liquid layer trapped between the vapour and heater surface and wall temperature could reach the Leidenfrost value. Authors proposed the following boiling crisis mechanism in the slug flow regime: the CHF was caused by a hot spot formation in the liquid film during the passage of a vapour clot along the channel. The formation of a hot spot on the heater surface was due to the liquid film disruption caused by nucleating bubbles in the liquid film.

Mattson, Hammitt and Tong [7] studied the subcooled flow boiling thermal crisis with Freon R113. They used a rectangular tests section ($7.35 \times 18.4\ mm^2$, 724 mm in heated length) with coolant velocity in the range 1–3.5 $m \cdot s^{-1}$ and pressure in the range 0.7–2.4 MPa. The authors obtained photographs and movie at 6 000 and 24 000 fps of flow pattern at increasing values of heat flux up to CHF. They obtained observations on flow pattern characteristics and vapour bubble motion, and measured bubble size. At thermal crisis condition, the flow pattern was characterised by the presence of a thin vapour layer on the heater surface and a bubble boundary layer.

Recently, Celata et al. [8] performed visualised CHF tests using water in subcooled flow boiling with an annular test section ($D_h = 5.75$ mm, heated length $Z =$ 100 mm). They obtained video sequences of flow patterns in subcooled flow boiling up to burnout in the pressure

range 0.1–1.1 MPa and with coolant velocity in the range 1–7.5 $m \cdot s^{-1}$. They reported flow pattern observations at different heat fluxes up to the CHF, together with several measured bubble parameters. Authors observed that, at boiling crisis conditions, vapour bubbles were rooted to the heated wall, and flow pattern changed with different water subcooling. Very few bubbles were entrained by the coolant stream. They also included some observations on the hot spot behaviour during the burnout.

As mentioned above, there are relatively few experimental works on flow visualisation at the CHF, which do not allow a clear insight into the boiling crisis mechanisms. In particular, the lack of direct observations of boiling phenomena correlated with the knowledge of bubble parameters measurements and wall temperature excursions, does not allow to clarify the actual events sequence for increasing heat flux values up to the CHF.

The objective of the present work is to perform a photographic study of the burnout in highly subcooled flow boiling, in order to provide a qualitative description of the flow pattern under different conditions of the boiling regime: ONB (onset of nucleate boiling), fully developed subcooled flow boiling and thermal crisis. Besides, vapour bubble parameters measurement associated with the wall temperature measurement will be provided for all boiling regimes, especially during the boiling crisis.

2. EXPERIMENTAL APPARATUS AND TEST PROCEDURE

The high speed photographic study of burnout in water subcooled flow boiling has been performed using the water loop, already extensively described in Celata et al. [9] shown in *figure 1*, while the optical equipment is schematically drawn in *figure 2*.

The loop, made of type 304 stainless steel and filled with deionized water, consists of the following components: main alternative pump, damper, filter, turbine flow meter, heated test section and water cooled tank. The test section is vertically oriented with water flowing upwards. It has been designed to obtain images of the flow boiling, over the surface of the heater, using a transmission method of illumination. The test section consists of two parts: the casing and the heater. In the casing we have a square duct flow channel. Two out of the four walls of the flow channel in the casing are made of Plexiglas, so that the light passes through these two transparent plates and illuminates the surface of the heater on which the boiling phenomena occur. The annulus has a square duct, the walls of which are respectively the two plates of Plexiglas

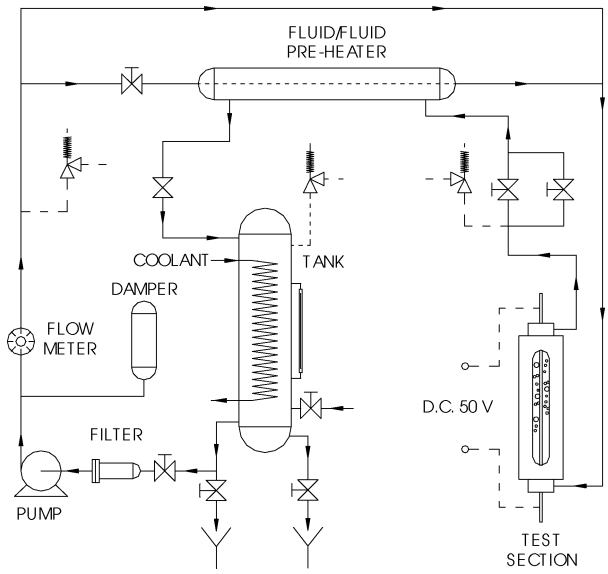

Figure 1. Schematic of the experimental facility.

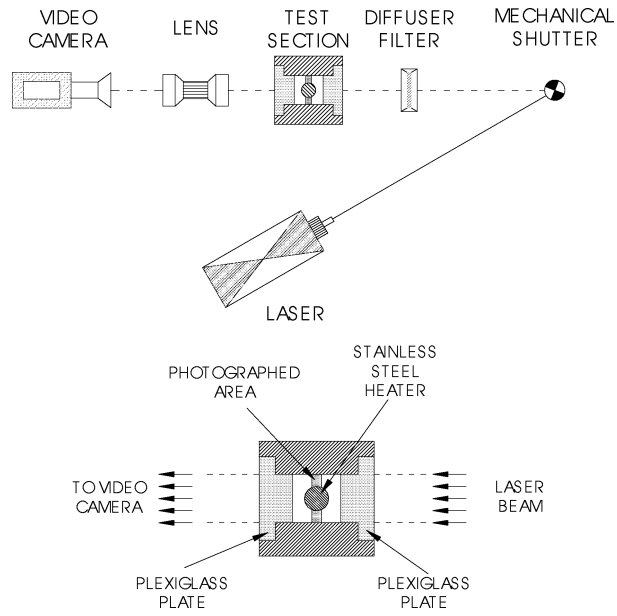

Figure 2. Schematic of the optical bench and detailed view of the flow channel.

and two stainless steel walls of the test section body, with a cylindrical heater (solid rod) at the centre of the square duct. The side dimension of the square duct is 7.2 mm. Dimensions of the cylindrical heater are 2 mm in diameter and 100 mm in length. The heater, one for each run, is made of stainless steel 316L type, and is uniformly heated over its length by Joule effect using an electric feeder up to 90 kW (50 V).

The bulk fluid temperature is measured just upstream and downstream of the test section using 0.5 mm K-type thermocouples, the latter after a suitable mixing of the fluid in order to ensure full condensation of all bubbles and therefore uniform temperature distribution. This makes the bulk exit temperature suitable for an energy balance in the fluid. The knowledge of the inlet and outlet temperatures, together with the measurement of the water mass flow rate, allows the computation of the thermal power delivered to the fluid by a heat balance in the coolant (calorimetric method). In this way heat losses from the test section are bypassed. All the parameters are continuously monitored using digital and analogue displays, and each variation is recorded. The experimental procedure consists in the following series of actions. The mass flow rate is set up using a manual control of the piston pump. Once the flow rate is steady, the thermal power is delivered to the test section. The control parameter used while approaching the CHF is the electrical power delivered to the test section, and the initial step in thermal power is 0.5 kW. Once 70 % of the expected CHF value is reached, the increment is reduced to 0.1 kW (from 0.1 to 0.6 % of the CHF). The expected CHF value is evaluated by previous experiments in channels with similar geometric conditions and same inlet conditions of the coolant. After each step, small adjustments in the flow rate are made, so that the exit flow conditions correspond to the desired ones. The above reported procedure is repeated until burnout occurs. The burnout is evidenced by the heater destruction and detected by the sharp drop in the electrical power reading.

The visualisation of the burnout was performed using the optical equipment shown in *figure 2*. Obtaining images of the burnout in subcooled flow boiling of water is complicated by various factors, such as:

- small size of vapour bubbles (< 0.1 mm);
- high flow velocity (up to 8 m·s^{-1});
- difficulty in defining the exact position of the burnout along the heater, associated with the very small portion of the heater interested by the light transmission due to the large image magnification required;
- impossibility in defining the exact instant of occurrence of the burnout.

In order to capture and "freeze" the motion of the vapour bubbles a 150 mW laser, as a light source, and a mechanical shutter were chosen. The mechanical shutter, which allows one to obtain a flash light lasting 1 μs, consists of a rotating mirror, with a vertical axis of rotation, which reflects the laser beam. The mirror is placed at an appropriate distance from the test section, in order that every point of the flow channel is illuminated by the light reflected for a period of 1 μs. The rotating speed of the mirror is regulated such as to obtain that a single frame recorded by the video camera corresponds to a single flash of the laser beam reflected in the mirror. After the reflection in the mirror, the laser beam passes through a diffuser filter, the flow channel, and a group of lenses, after which is captured by the video camera. A diffuser filter, constituted by a frosted glass, is placed between the test section and the rotating mirror, in order to reduce disturbances in video images due to the variation of the water refraction index caused by the presence of high temperature gradient in the liquid near the heater surface.

To take movies of the burnout occurrence, a CCD video camera, whose speed is 50 fps, and a VHS video recorder were chosen. In fact, for the occurrence of burnout one may wait for a period of time variable up to few minutes.

Because of the uniform heating, burnout occurs in the proximity of the exit section at the top of the heated channel, but its exact position is variable in the range of 3–5 mm below the exit section. Therefore, to capture a high quality video sequence of the burnout it is necessary to perform several tests at the same inlet conditions but at different value of the height of the plane containing the optical equipment, with 4 or 5 unsuccessful attempts for each condition. The images of burnout are analysed through a PC digital image processing system.

3. EXPERIMENTAL RESULTS

The summary of test conditions (liquid velocity and system pressure) for the present experimental campaign is given in *table I*. The inlet temperature for all tests is $T_{in} = 20\,^{\circ}$C. Only in tests marked by an "X", the burnout is successfully captured by the video camera, and under each mark there is the reference name of the test. This paper reports only the results of tests with $u = 3$ m·s^{-1} (test A2A) and $u = 5$ m·s^{-1} (tests E2A and E2D), because at higher velocities it was not possible to distinguish bubbles in the images. A larger image

TABLE I
Test conditions ($T_{in} = 20\,^{\circ}$C for all tests).

Pressure \ Velocity	3 m·s^{-1}	5 m·s^{-1}	7.5 m·s^{-1}	10 m·s^{-1}
5 bar	A2A X	E2A X		
10 bar		E2D X		
20 bar			F2Q X	
30 bar			F2S X	

magnification should solve this problem in the future work.

3.1. Wall temperature measurement

The heater wall temperature is obtained from the elongation of the heater rod for each heat flux step. A schematic of the heater elongation measurement system is drawn in *figure 3*. The heater rod is formed by three components: lower copper clamp, stainless steel (AISI 316L) rod and upper copper clamp. From the knowledge of AISI 316L, Touron [10], and copper thermal properties it is possible to evaluate the mean temperature of the stainless steel rod. The wall temperature is calculated using the conduction Fourier's law. The wall temperature obtained with this procedure is the mean value of the heater surface temperatures in the heated section. Nonetheless, once subcooled flow boiling spreads all along the channel, the heater temperature is almost flat, and its approximation with the average value obtained from the experimental apparatus would seem to be quite reasonable. The difference between the inlet and the outlet wall temperature calculated with the Shah [11] correlation for the heat transfer coefficient (for tubes and annuli) is less than 5 K. Therefore, it is reasonable to consider the wall temperature calculated with this method as a good approximation of the heater surface temperature before and at the thermal crisis occurrence. Before the onset of subcooled boiling, the heater wall temperature has a linear trend and the average value obtained from the measurements is compared with the average value of the wall temperature. *Figures 4–6* show the heater wall temperature as a function of the heat flux at a given inlet subcooling and mass velocity for our experimental tests. Besides, the graphs show the wall temperature calculated with Shah [11], Thom [12] and Jens and Lottes [13] correlations, for the subcooled flow boiling region, as a function of the heat flux. The temperature calculated with these correlations is the mean temperature between inlet and outlet section of the flow channel. In this way, the calculated temperature can be compared with the wall

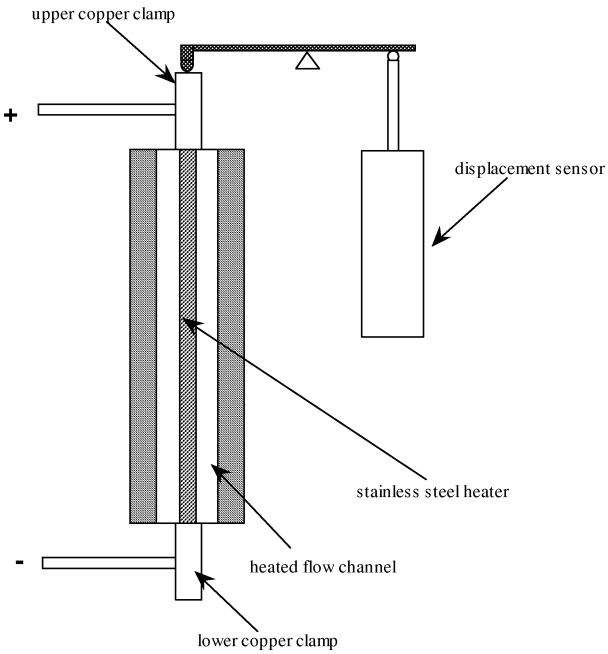

Figure 3. Schematic representation of the heater elongation measurement system.

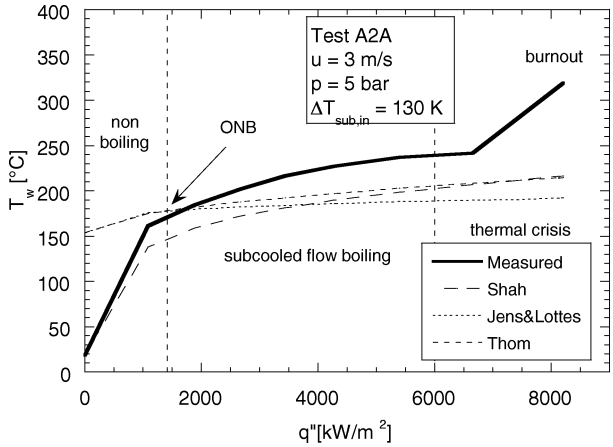

Figure 4. Wall temperature as a function of heat flux for test A2A.

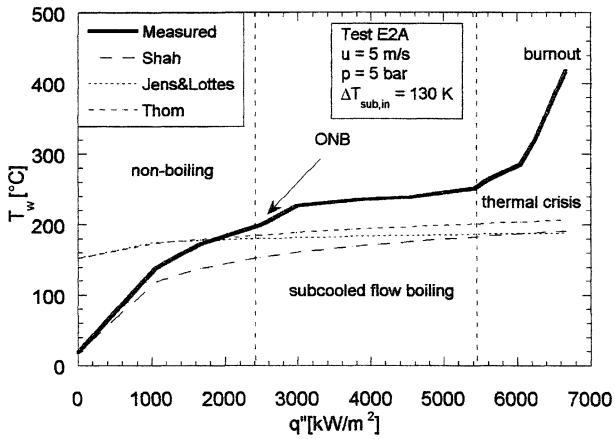

Figure 5. Wall temperature as a function of heat flux for test E2A.

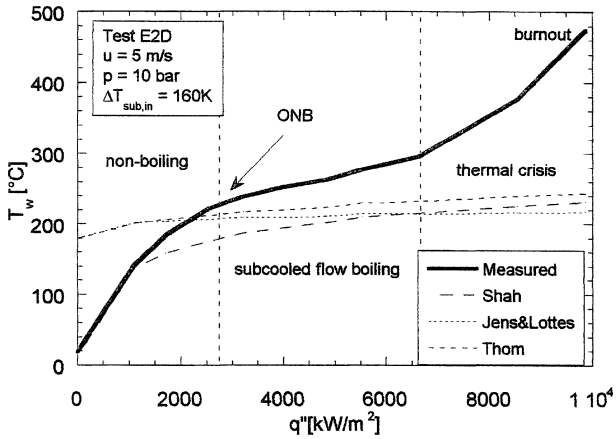

Figure 6. Wall temperature as a function of heat flux for test E2D.

temperature evaluated from the heater rod elongation measurement. The graphs are divided in two different heat transfer regions: single-phase and subcooled flow boiling.

The separation line between the two regions gives the onset of nucleate boiling heat flux, q''_{ONB}, calculated with the Bergles and Rohsenow [14] correlation. This calculated value is generally overestimated with respect to the heat flux at which first vapour bubbles appear in the images of the flow channel. In the single-phase region there are few experimental points and the wall temperature curves are almost linear. As soon as the heat flux is higher than the q''_{ONB}, the nucleation occurs on the heater and the graphs show a sensible reduction in the T_w slope. In this region the wall temperature curves are quite "flat" as expected, and a large increase in the heat flux produces a small increase in the surface temperature. Over a certain heat flux value the wall temperature sensibly changes its slope. This is the boundary between the subcooled flow boiling region and the thermal crisis region. Thermal crisis produces a reduction in the heat transfer between the heater surface and the coolant with the notable increment of the wall temperature, being the heat flux constant. In this region each heat flux increment corresponds to an increase in the wall temperature until the heater burnout at 1 400 °C. In the graphs, the measured wall temperature never reaches the melting temperature of the stainless steel. In fact, the reported wall temperature is averaged over the entire heated length. During the burnout, only a small portion of the heater surface reaches 1 400 °C, being the rest of the surface at a temperature typical of the subcooled flow boiling regime. Therefore, the mean value of this temperature distribution is quite far from 1 400 °C.

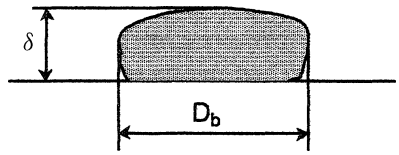

Figure 7. Vapour bubble parameters (δ = height, D_b = length or diameter).

Generally, in the subcooled flow boiling region the wall temperature reported in the graphs is about 40–50 K higher than the temperature calculated using the heat transfer coefficient correlations of Shah [11], Thom [12] and Jens and Lottes [13]. This discrepancy should depend on the approximation introduced in the procedure for the wall temperature calculation, based on the elongation of the heater rod. In any case, the comparison of the wall temperature with the calculated values, is aimed to verify the T_w calculation procedure. Although the approximation of the wall temperature calculation is not accurate, for the purposes of this work is quite sufficient. The qualitative knowledge of the heater temperature is very important. In fact, the analysis of the T_w–q'' curves, joined with images of bubbles formation, provides useful information about the thermal crisis mechanisms. In particular, the knowledge of the CHF occurrence, determined by the second slope change in the T_w–q'' curves, allows us to focus the images analysis only in the video-sequences relative to the thermal crisis region. In the works performed in the past (Gunther [1], Kirby et al. [2–4] Mattson et al. [7], van der Molen and Galjee [5]) the absence of the wall temperature information was a limitation to understand the physical phenomena preceding the heater burnout.

3.2. Bubble parameters measurements

Figure 7 reports the geometrical parameters of vapour bubbles measured from video images where D_b is the bubble diameter or length, and δ is the distance from the heater surface to the top of the bubble (height). The measurement of bubble parameters is obtained for each heat flux value until burnout occurring. Graphs of *figures 8–10* show the results of vapour bubble measurements for three different runs.

Due to the random nature of boiling, parameters of vapour blanket (i.e. elongated bubbles due to small bubbles coalescence) are measured from video images on the ground of the following argumentation. Images consist of a sequence of frames 20 ms spaced. As the boiling cycle of a single vapour bubble lasts less

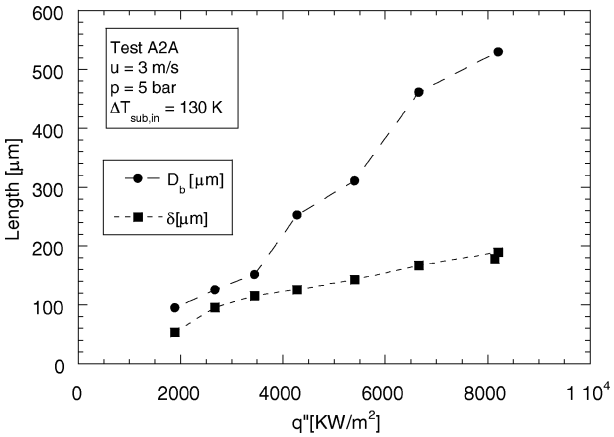

Figure 8. Measured vapour bubble parameters for test A2A.

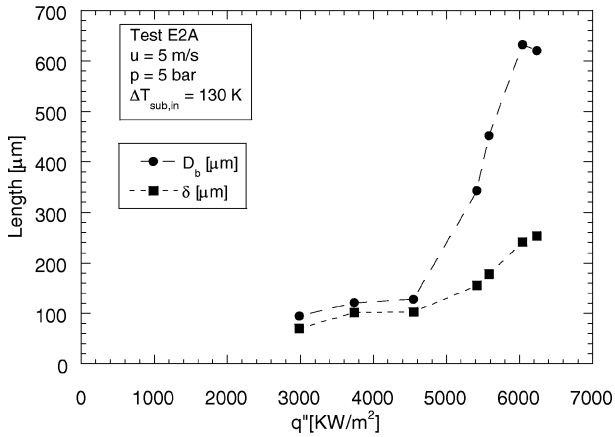

Figure 9. Measured vapour bubble parameters for test E2A.

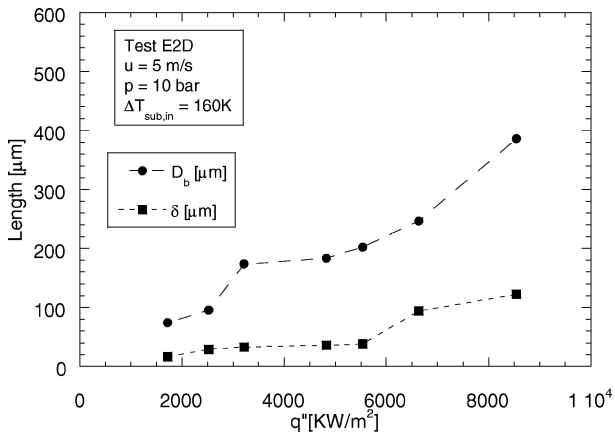

Figure 10. Measured vapour bubble parameters for test E2D.

than 20 ms (Bibeau and Salcudean [15]) and as active microcavities have variable waiting periods, each frame shows the situation of the heater surface in a random instant of the boiling cycle. The largest vapour bubbles present in the frames are measured. In this way, it is reasonable to consider that the measured dimensions of the bubbles represent the maximum reachable under those conditions. The values reported in graphs are the average among measurements obtained from different images at the same heat flux. From the graphs it is possible to see the heat flux effect on D_b and δ for different coolant velocity and system pressure. When the heat flux is increased, D_b and δ clearly increase and reach values from 3 to 6 times the initial one. Bubble length is 2–3 times larger than the bubble height. Considering the present test conditions, i.e. the high degree of subcooling ($\Delta T_{sub,in} > 100$ K), most of vapour bubbles normally do not detach from the heater surface. In fact, video images show very few bubbles detaching from the wall and carried by the coolant stream.

From video images it is not possible to obtain information regarding the vapour bubble motion along the flow channel as described by Bibeau and Salcudean [15]. Authors reported in detail the sliding of a vapour bubble on the heated wall in subcooled flow boiling of water from the nucleation up to the detachment. According to the authors, vapour bubbles slide along the heater wall during the growth period and this phenomena starts immediately after nucleation.

3.3. Flow pattern observations

This section reports the qualitative descriptions of the flow pattern observed during the experiments. Flow pattern observations are obtained from the analysis of flow boiling images recorded by the video camera at different values of heat flux from the ONB up to the CHF. Several types of observations are collected and reported: vapour bubble shape, bubble contour type (regular or irregular), presence of detached bubbles, hot spot appearance, etc. All these qualitative information are then collected and grouped in several flow regimes called: *microbubbles*, *isolated bubbles*, *coalesced bubbles* and *large bubbles*.

Microbubbles. When the heat flux exceeds the q''_{ONB} value, it is possible to observe the presence of very small vapour bubbles on the heater surface (*figure 11*). Such kind of bubbles is characterised by quite small dimensions ($D_b < 40$ μm). With the enlargement adopted presently it is impossible to measure on the video a length less than 40 μm with reasonable accuracy.

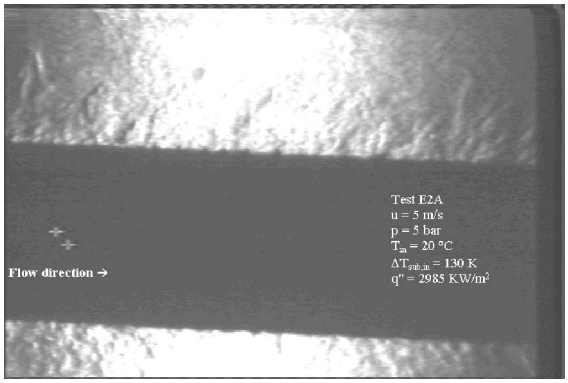

Figure 11. Microbubble flow pattern.

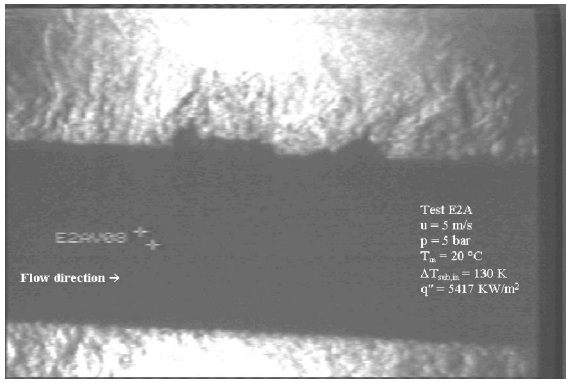

Figure 13. Coalesced bubble flow pattern.

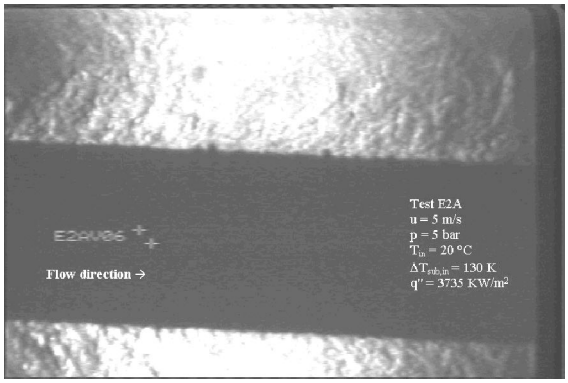

Figure 12. Isolated bubble flow pattern.

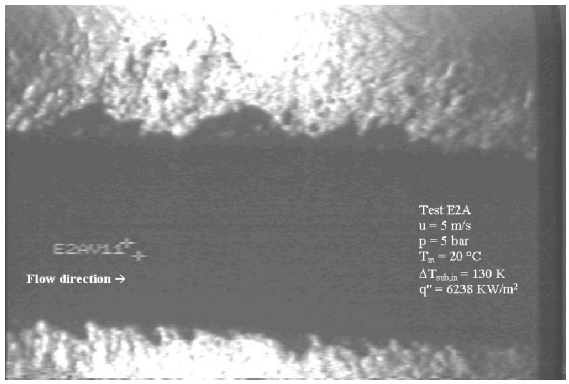

Figure 14. Large bubble flow pattern.

Isolated bubbles. As the heat flux is increased, dimensions of vapour bubbles increase and the bubble maintains an elliptical shape (*figure 12*). In this region, any further heat flux increase produces a clear increase in bubble diameter and height, as well as in the number of bubbles. Most vapour bubbles observed are attached to the heater surface. Occasionally very few bubbles detach from the wall and are carried by the coolant.

Coalesced bubbles. For a given value of heat flux, some vapour bubbles begin a sort of transversal coalescence (*figure 13*). As bubbles increase their diameter, they interfere with the neighbour bubbles and produce coalesced bubbles. These bubbles are larger than the former ones, but maintain the same shape (elliptical or hemispherical) with regular and smooth contour.

In images obtained with the current optical facility, the vapour bubble motion is frozen by a flash light of 1 μs of duration. This means that from frames recorded by the video camera, no information on bubble velocity may be extrapolated. In particular, slipping bubbles (as reported by Bibeau and Salcudean [15]) on the heater surface are not observable.

In the *microbubbles*, *isolated bubbles* and *coalesced bubbles* regions the wall temperature has a low slope, the heat flux having a weak influence on it, which is typical of the subcooled flow boiling regime.

Large bubbles. In this region the flow channel is characterised by the presence of large size vapour bubbles (*figure 14*). Bubble dimensions start to increase in diameter and height. Bubble contour and shape are irregular. At low pressure (3 bar for our tests) in some pictures we may observe as most of the heater surface is covered by such kind of large bubbles, and in some cases bubbles are stretched by the coolant stream.

In the *large bubbles* region, during the heat flux increments a bright red hot spot, typical of white-hot metals, appears on the heated wall and after a period of time depending on test conditions, the burnout of the heater occurs (*figure 15*). In *figure 18* the hot spot is placed on the right of the picture. The burnout is

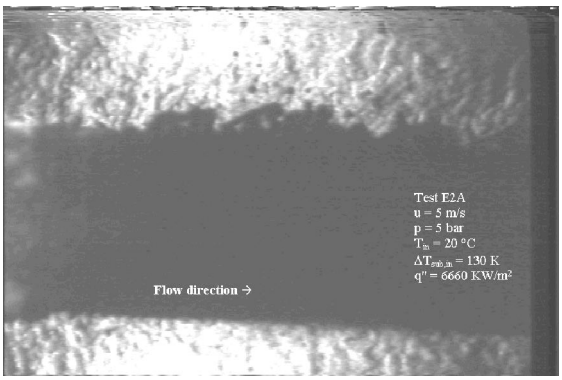

Figure 15. Burnout occurrence.

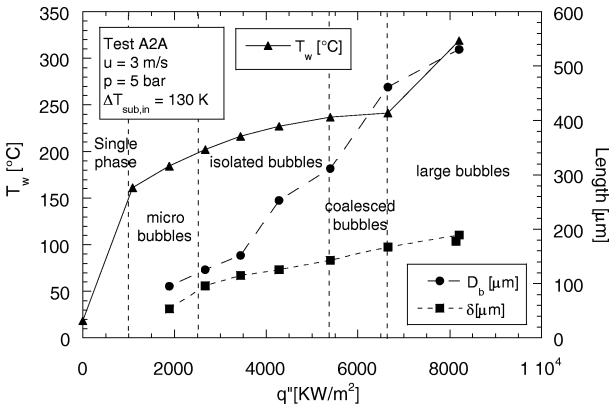

Figure 16. Measured wall temperature and vapour bubble parameters versus heat flux for test A2A.

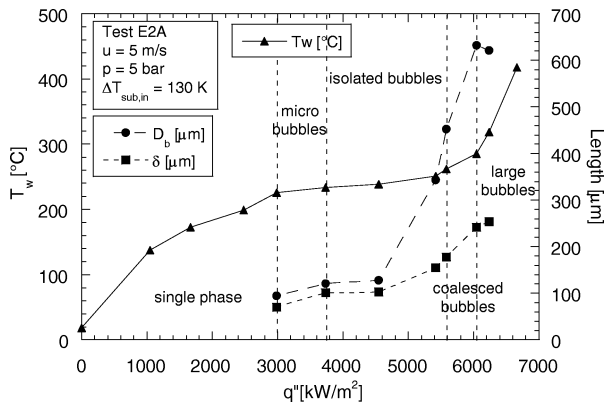

Figure 17. Measured wall temperature and vapour bubble parameters versus heat flux for test E2A.

characterised by a sudden rupture of the heater, with a light flash. The hot spot indicates that the temperature of the heated wall has reached approximately the value of 700–800 °C. The hot patch lasts for a period of time

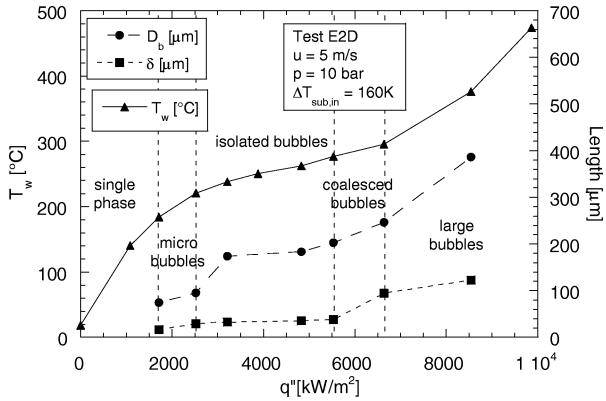

Figure 18. Measured wall temperature and vapour bubble parameters versus heat flux for test E2D.

variable from few milliseconds up to few seconds. During the existence of the hot spot, the temperature of the heater is increased up to 1 400 °C (melting point for AISI 316L). The hot spots appear suddenly during the waiting period after each microincrement of the heat flux. The appearance of the first hot spot on the surface of the heater indicates that the boiling crisis is already being established.

In the images preceding the appearance of the first hot spot it is possible to observe an interesting boiling behaviour at the heater surface. In the few milliseconds preceding the appearance of the hot spot, the heater surface is interested by a *reduced boiling activity*. There are very few vapour bubbles, most of images showing a clean heater surface without any vapour bubble. This phenomenon was also observed in previous visual experiments described by Celata et al. [8].

The *reduced boiling activity* is also observed on the heater wall during the period of existence of the hot spot. Vapour bubble formation is almost absent on the surface with the highest temperature (the portion that emits the red light). Occasionally, some isolated bubbles are observed. A very high intensity boiling occurs on the area just near the boundary between the hot spot and the rest of surface with a lower temperature (*figure 15*).

3.4. Summary graphs and events sequence from ONB up to CHF

In the previous sections, three types of information, wall temperature measurement, vapour bubble parameters measurement and qualitative flow pattern observation, have been reported and discussed. Each type of information gives a partial view of the boiling phenomena

and does not allow understanding the mutual interactions among heater temperature, heat flux, vapour bubble dimensions and flow pattern. Therefore, in order to obtain a global point of view of the complex phenomena occurring on the heater surface from the ONB up to the CHF, all measured parameters as well as observed flow patterns are collected together in graphs, as a function of heat flux, in *figures 16–18*. From these graphs it is possible to highlight the following points based on experimental evidences:

1. From the *onset of nucleate boiling*, increasing heat flux values produce an increase in bubble dimensions (length and height) as well as in bubbles population. This latter effect is due to the increase of active nucleation sites on the heater surface.

2. In subcooled flow boiling, the heat flux has a weak influence on the heater wall temperature.

3. For a given value of the heat flux, wall temperature curve changes its slope and its value increases with increasing the heat flux.

4. The wall temperature slope change occurs during the *coalesced bubbles* or *large bubbles* flow regimes.

5. During the *large bubbles* flow regime a hot spot appears on the heater surface and after few milliseconds the burnout occurs with the consequent heater rupture.

4. BURNOUT MECHANISM

The main purpose of this work is to attain a good understanding of the phenomena causing the thermal crisis and the relative burnout in subcooled flow boiling of water. This section is an attempt to explain the experimental observations reported in the previous section. In *figures 16–18* it is possible to observe the behaviour of the wall temperature in the *coalesced bubbles* and *large bubbles* regions. In these regions, there is an abrupt increase in the T_w slope with increasing the heat fluxes until the hot spot appearance. Therefore, it would seem that the presence of large bubbles associated with higher heat fluxes on the heater surface causes relevant wall temperature increment.

In subcooled flow boiling of water in channels, increasing heat flux values produce, from the *onset of nucleate boiling* (ONB), an increase in bubble dimensions (length and height) as well as in bubbles population. This latter effect is due to the increase of active nucleation sites on the heater surface. For sufficiently high heat flux, vapour bubbles are quite large and flat with an irregular contour. In this situation, the thin liquid layer adsorbed

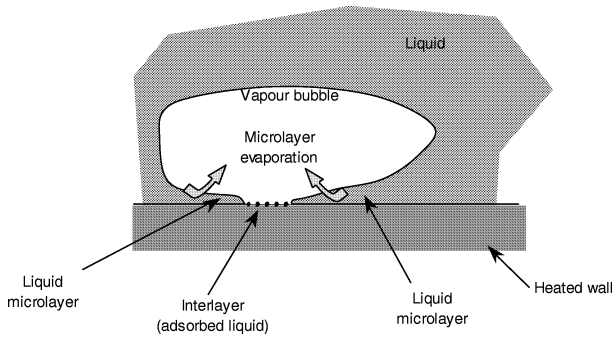

Figure 19. Schematisation of a vapour bubble.

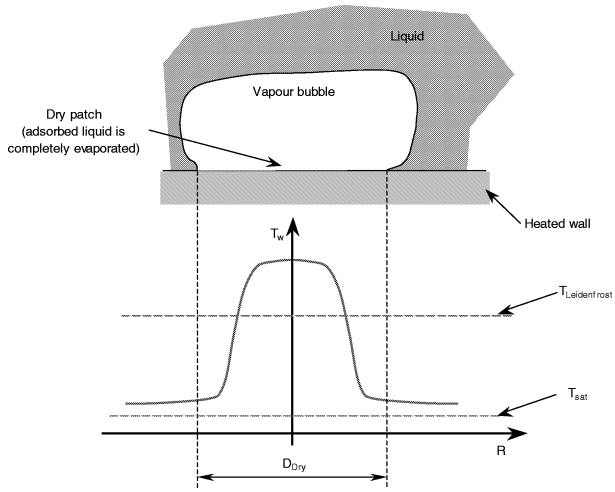

Figure 20. Schematisation of dry patch formation under a vapour bubble.

on the heater surface at the bubble base during nucleation (*figure 19*) evaporates completely and leaves a dry patch under the bubble (Straub [16]). Therefore, on that portion of the heated surface covered by the dry patch, under the vapour bubble, wall temperature increases and causes further evaporation of the liquid microlayer (*figure 20*). In *figure 20* this phenomenon is reported schematically and the temperature graph is qualitative.

Generally if the wall temperature at the bubble base is lower than the Leidenfrost limit, dry patches eventually formed at the bubble base should be rewetted after the bubble collapse by the cold liquid surrounding the bubble and the wall temperature should drop off. This continuous formation and destruction of dry patches on the heater surface produces two effects on the wall temperature: large fluctuations, as reported by Fiori and Bergles [6], and increase in average values. The latter effect, the average increase of the wall temperature, is

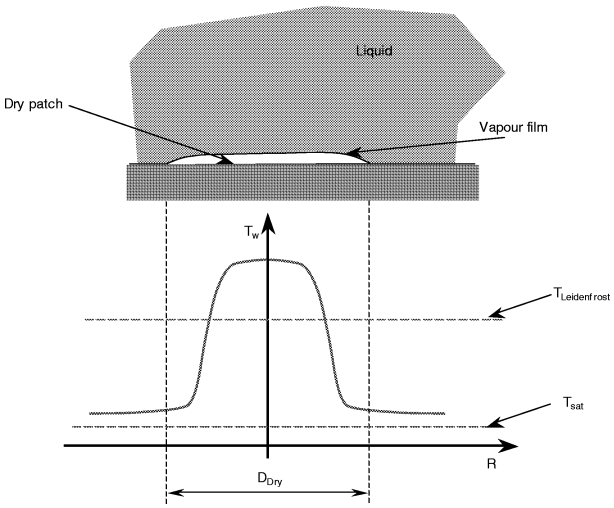

Figure 21. Schematisation of the stable dry patch formation.

represented in *figures 16–18* by the wall temperature slope increase.

On the other hand, for sufficiently high heat fluxes, the wall temperature at the bubble base can reach the Leidenfrost value and after the bubble collapse the dry patch is not rewetted by the liquid, and it remains covered by a thin, stable vapour film (*figure 21*). Stable vapour film can survive only if its area is sufficiently large in order to maintain the wall temperature well above the Leidenfrost limit. After the bubble collapse, the surface covered by the vapour film on the dry patch is cooled by the lateral conduction in the heater material while the cool liquid cannot wet directly the heater surface due to the presence of the vapour film. For sufficiently large dry patch, the thermal conduction is not able to cool the portion of the heater under the dry patch and, therefore, the wall temperature remains above the Leidenfrost limit. This is the beginning of the thermal crisis. During the existence of the stable vapour film on the heater surface, the heat transfer, between the heater and the liquid, is reduced due to both thermal insulation and nonboiling. On the insulated surface, the wall temperature rises up to its melting point, resulting in the burnout.

Another important experimental observation is the so-called *reduced boiling activity*. This phenomenon occurs during the presence of *large bubbles* and precedes the hot spot appearance. The *reduced boiling activity* can be explained in the following way. The stable dry patch prevents the contact between heater surface and water and the nucleation sites on the heater surface to be rewetted by the liquid.

Therefore, the combination of these two effects, insulation and nonboiling, causes the dramatic reduction in the heat transfer coefficient, typical of the thermal crisis. At this stage, the wall temperature increases from the Leidenfrost value (indicatively in the range 250–300 °C) up to the hot spot appearance (800–900 °C) and then to the heater burnout (1 400 °C). Typical thickness of the vapour film should be very small, approximately less than 10 μm. This value is also given by a simple calculation obtained using the heat transfer equation between the heater surface covered by a vapour film and the liquid bulk:

$$q'' = k_v \frac{T_w - T_l}{\delta_v} \qquad (1)$$

where k_v is the vapour thermal conductivity. Heat transfer is governed principally by heat conduction from the wall to the liquid, through the thin vapour film of thickness δ_v. Equation (1), with $k_v = 0.318701 \cdot 10^{-4}$ kW·m^{-1}·K^{-1} (at $p = 5$ bar), $T_l = 28$ °C, $T_w = 900$ °C and $q'' = 6\,000$ kW·m^{-2}, gives for δ_v the value of 4.63 μm, which confirms the above visual observation.

In video images taken during the *reduced boiling activity* it is not possible to verify by direct observation the presence of any vapour film. The vapour film existence can be proved only through the following observations. During the hot spot occurrence it would seem that the coolant be in contact with the heater surface at a temperature of 900–1 200 °C. In this situation, neither nonboiling activity nor vapour film are observed on the surface of the hot spot. As liquid water cannot be maintained in metastable equilibrium with such a high superheated surface, it is reasonable to suppose the existence of an insulating vapour layer in order to keep separated the high temperature wall and the subcooled liquid. Besides, the same observation can be applied during the *reduced boiling activity* when the wall temperature is in the range 300 °C (Leidenfrost)–900 °C (white-hot metal). Therefore, according to the above argumentation, the liquid film should be formed during the *reduced boiling activity* up to the physical heater burnout. The vapour film presence during the *reduced boiling activity* is consistent with the film boiling heat transfer regime described by Fiori and Bergles [6] before the burnout occurrence. In fact, they indicated the stable film boiling as the region where the measured wall temperature had steadily increasing values.

Regarding the value of the Leidenfrost temperature, it is not possible to predict an appropiate value. Therefore, it is possible to consider a reasonable Leidenfrost temperature in the range of 250–300 °C, which corresponds to a superheating of 100–150 K for water at 0.5 MPa

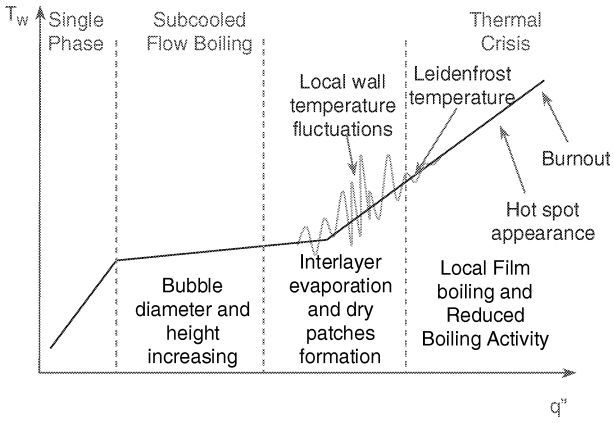

Figure 22. Schematisation of the events sequence leading to the heater burnout.

($T_{sat} = 151\,°C$). In any case, Lienhard [17] showed that the thermodynamic limit of liquid superheat ΔT_{tl} can be calculated with the following equation:

$$\frac{\Delta T_{tl}}{T_{crit}} = 0.905 - \frac{T_{sat}}{T_{crit}} + 0.095\left(\frac{T_{sat}}{T_{crit}}\right)^{8} \qquad (2)$$

where $\Delta T_{tl} = T_{tl} - T_{sat}$, T_{crit} is the critical temperature of water ($T_{crit} = 374.15\,°C$) and T_{sat} is the water saturation temperature. Equation (2) for the test at 5 bar ($T_{sat} = 151.87\,°C$) gives $T_{tl} = 312\,°C$. This could be considered as the upper limit of the Leidenfrost temperature, because water cannot exist in liquid metastable state for a higher superheating.

At this point it is possible to draw the events sequence that precedes the burnout of the heater according to the schematisation of the *figure 22*. During the subcooled flow boiling regime, for increasing heat flux values, vapour bubbles increase their dimensions (height and diameter) and their population. This flow regime corresponds to the observed *microbubbles* and i*solated bubbles* conditions above reported. Wall temperature slope is quite low and is typical of the subcooled flow boiling region. When the heat flux reaches a particular value, vapour bubbles start their transversal coalescence and for further heat flux increments, *large bubbles* appear in the flow channel. The wall temperature is now dependent on the heat flux and its slope is high. Under these conditions, dry patches are continuously formed and destroyed under bubbles with large fluctuations in the wall temperature. If the wall temperature reaches the Leidenfrost value (250–300 °C) in a large portion of the heater surface, dry patches would not be rewetted by the coolant after the bubble collapse. This is the beginning of the boiling crisis phenomena. Any further heat flux increment produces a heater surface temperature increase and an extension of the dry area covered by a thin vapour film. This stage corresponds to the *reduced boiling activity* region above reported. For a given heat flux, surface temperature reaches 800–900 °C and a bright red hot spot appears on the heater and after few seconds the physical burnout occurs.

5. CONCLUSIONS

High speed movies of the flow pattern in water subcooled flow boiling, from the onset of nucleate boiling up to the physical burnout of the heater, are recorded. Bubble dimensions are derived from images and reported as a function of the heat flux for three different thermal hydraulic conditions. Also, the heater wall temperature is measured and reported in graphs. The video image analysis allows a qualitative description of the near wall flow patterns for increasing values of the heat flux up to the CHF. Bubble parameters and wall temperature measurements, as well as direct observations of flow patterns, for all flow regimes, are reported in summary graphs witch provide a detailed description of the phenomena from the boiling crisis up to the heater burnout. Conclusions of the visualised study can be summarised as follows:

1. Bubble shape and dimensions (diameter and height) are a function of the heat flux.

2. During subcooled flow boiling, the heat flux has a weak influence on the wall temperature.

3. When the flow pattern is characterised by the presence of large bubbles, the wall temperature is strongly influenced by the heat flux up to the heater burnout.

4. Before the hot spot appearance, the heater surface is characterised by a *reduced boiling activity*.

5. On the hot spots the bubbles formation is almost inhibited.

From the analysis of the experimental observations, it is possible to deduce the thermal crisis mechanisms. During nucleation in subcooled flow boiling, at sufficiently high heat flux, the thin liquid layer adsorbed on the heater surface at the bubble base during nucleation, evaporates completely and leaves a dry patch under the bubble. After the bubble collapse, if the heater surface temperature reaches the Leidenfrost value, the dry patch is not rewetted by the liquid, and it remains covered by a thin, stable vapour film. During the existence of the stable vapour film on the heater surface, the heat transfer, between the heater and the liquid, is reduced due to both thermal insulation and nonboiling. On the insulated surface, the wall

temperature rises up to its melting point, resulting in the burnout.

REFERENCES

[1] Gunther F.C., Photographic study of surface-boiling heat transfer to water with forced convection, Trans. ASME 73 (1951) 115–121.

[2] Kirby G.J., Stainforth R., Kinneir J.H., A visual study of forced convection boiling. Part 1. Results for a flat vertical heater, Atomic Energy Establishment Winfrith, AEEW-R 281, 1965.

[3] Kirby G.J., Stainforth R., Kinneir J.H., An investigation into a possible mechanism of subcooled burnout, Atomic Energy Establishment Winfrith, AEEW-M 725, 1967.

[4] Kirby G.J., Stainforth R., Kinneir J.H., A visual study of forced convection boiling. Part 2. Flow patterns and burnout for a round test, Atomic Energy Establishment Winfrith, AEEW-R 506, 1967.

[5] Van der Molen S.B., Galjee F.W.B.M., The boiling mechanism during burnout phenomena in subcooled two-phase water flows, in: Heat Transfer, 1978, Paper FB-19, pp. 381–385.

[6] Fiori M.P., Bergles A.E., Model of critical heat flux in subcooled flow boiling, in: Heat Transfer, Vol. 4, 1970, Paper B-6.3.

[7] Mattson R.J., Hammitt F.G., Tong L.S., A photographic study of the subcooled flow boiling crisis in freon 113, in: ASME-AICHE Heat Transfer Conference, Atlanta, August 5–8, 1973.

[8] Celata G.P., Cumo M., Mariani A., Zummo G., Preliminary remarks on visualisation of high heat flux burnout in subcooled water flow boiling, in: G.P. Celata, R.K. Shah (Eds.), Two-phase Flow Modelling and Experimentation, Vol. 2, Edizioni ETS, 1995, pp. 859–872.

[9] Celata G.P., Cumo M., Mariani A., Burnout in highly subcooled flow boiling in small diameter tubes, Int. J. Heat Mass Tran. 36 (1991) 1269–1285.

[10] Touron H., Initial design equation for 316L austenitic steel, Final Report N. 169/84–9/FU/NET, CEA, 1985.

[11] Shah M.M., Generalized prediction of heat transfer during subcooled flow boiling in annuli, Heat Tran. Engrg. 4 (1983) 24–31.

[12] Thom J.R.S., Walker W.M., Fallon T.A., Reising G.F.S., Boiling in subcooled water during flow up heated tubes or annuli, in: Proc. Symp. on Boiling Heat Transfer in Steam Generation Units and Heat Exchangers, Manchester, 1965, Paper 6.

[13] Jens W.H., Lottes P.A., Analysis of heat transfer burnout, pressure drop and density data for high pressure water, ANL Report, ANL-4627, 1951.

[14] Bergles A.E., Rohsenow W.M. (1963), The determination of forced convection surface boiling heat transfer, in: ASME-AIChE US National Heat Transfer Conference, Boston, 11–14 August, 1963, Paper 63-HT-22.

[15] Bibeau E.L., Salcudean M., A study of bubble ebullition in forced-convective subcooled nucleate boiling at low pressure, Int. J. Heat Mass Tran. 37 (1994) 2245–2259.

[16] Straub J., The role of surface tension for two-phase heat and mass transfer in the absence of gravity, Experimental Thermal and Fluid Science 9 (1994) 253–273.

[17] Lienhard J.H., Correlation for the limiting liquid superheat, Chem. Engrg. Sci. 31 (1976) 847–849.